THE URFT MASONRY DAM,

THREEDIMENSIONAL STABILITY ANALYSES, MONITORING AND COMPARISON OF RESULTS

Walter Wittke
Prof. Dr.-Ing. W. Wittke, Geotechnical Consultants,
Henricistrasse 50, D-52072 Aachen,
Phone: +49 241 88987-0
Fax: +49 241 88987-33

Dipl.-Ing. Herbert Polczyk
Wasserverband Eifel-Rur
Eisenbahnstraße 5, D-52321 Düren,
Phone: +49 2421 494-13 50

1. Introduction

The Urft dam, with a height of 58 m and a width at the foundation level of approximately 65 m, was built from 1900 until 1904 according to Prof. Intze's plans. It is curved towards the upstream side, and the 226-metre-long dam crest has a curvative with a radius of 200 m (fig. 1).

Since the heightening of the Rur dam Schwammenauel in 1959, the Urft dam has a pondage of 12 m on it's downstream side.

Fig. 1: Urft Reservoir

Lime efflorescences on the downstream face of the dam in 1980 gave rise to carry out an extensive drilling and investigation programme in order to determine the substance of the dam and the foundation rock. After this programme had provided satisfying results, the dam's stability could preliminarily be proven by three-dimensional finite element analyses. For a conclusive assessment of the stability, however, as well as for an adjustment of the dam to the generally acknowledged technical standards, an appropriate remediation programme had to be developed and submitted to the supervising authority.

Most important elements of the rehabilitation measures were the excavation of two inspection galleries by blasting and the installation of a monitoring programme (fig. 2). Moreover, Lugeon, dilatometer and flat jack tests have been carried out in order to determine the permeability and deformability of the dam and the foundation rock. The reservoir level could not be lowered during execution of these works.

2. Wall and Foundation Rock

Figure 3 shows the geological conditions in the area of the masonry dam. The rock masses belong to the upper Rurberger layers of the Lower Devonian. There are massive sandstone layers as well as alternating sequences of silt, sand- and clay-stone layers at the left slope, whereas silt and clay-stones are prevailing in the middle of the valley. The right hillside mostly consists of alternating sequences of silt and sandstone layers.

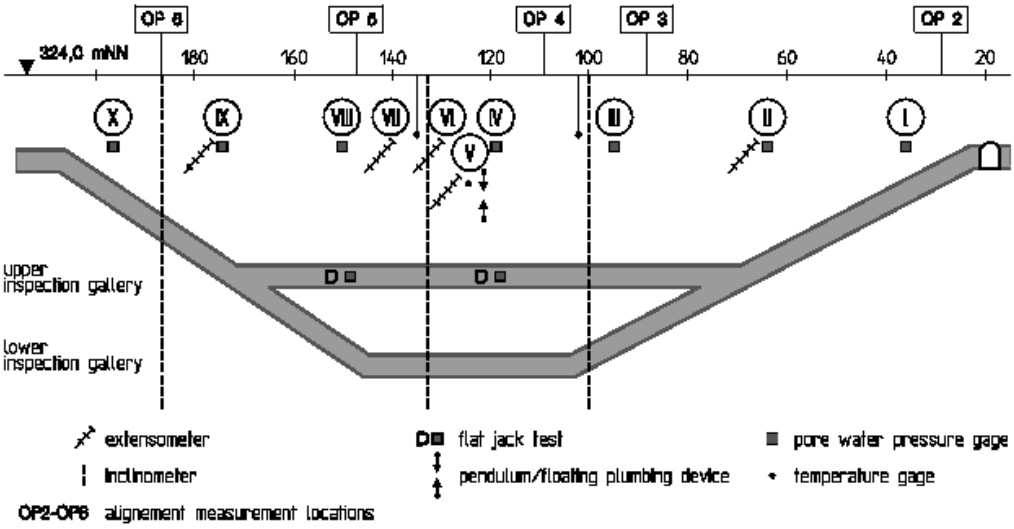

Fig. 2: Measuring Devices and Locations (Longitudinal Section)

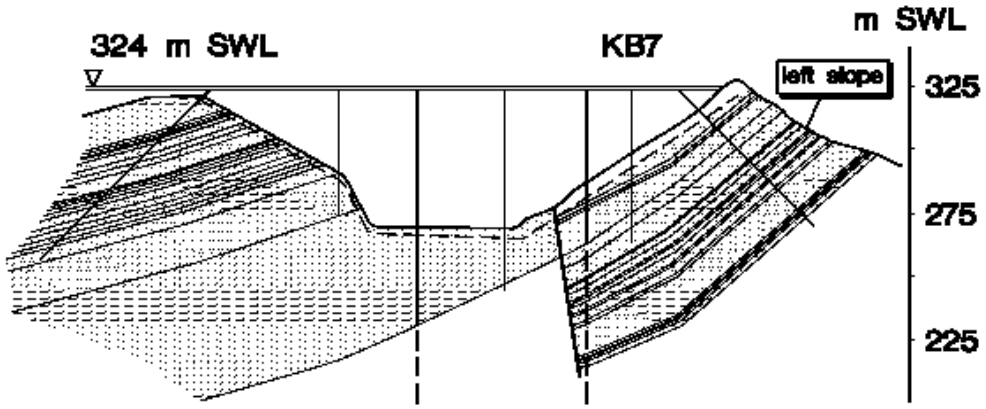

Fig. 3 Geological section

The orientation of the families of discontinuities, which are important for the stability of the dam and the permeability of the underlying rock are shown in figure 4.

A more precise knowledge of the composition of the foundation rock and the concrete dam was to be gained with the aid of core drillings. In the following the essential results gained from all core drillings are illustrated on the basis of drilling KB 7.

Drill cores, obtained from this core drilling, are shown in fig. 5 for the masonry. It consists mainly of greywacke rubble stones, which are embedded in a mortar of lime-trass-concrete. The mortar is in good condition and shows no leaching

damage, which is probably due to it's high lime content. This high lime content led to efflorescences on the wall's downstream face.

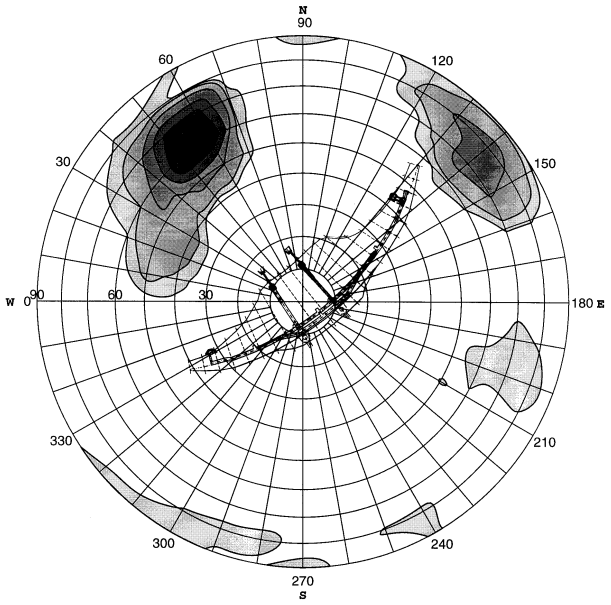

Fig. 4: Discontinuity fabric

Lugeon tests have shown low coefficients of permeability for the masonry. In drilling KB 7 a k_f-parameter ranging from 10^{-6} up to 10^{-7} m/s was determined. Higher coefficients of permeabilities, however, accur adjacent to the foundation. Dilatometer tests, which have been carried out in the masonry, have led in case of KB 7 to Young's moduli reaching from 3000 MPa to 6000 MPa. These values are within the expected range.

The cores further reveal sandstones, prevailing down to a depth to 40 m. These are followed by alternating sequences of sand- and clay-stones and layers, mainly consisting of clay-stones, which commence in a depth of approx. 50 m.

Lugeon tests have shown that the permeability is becoming smaller with greater depth. Only small permeabilities, in the order of $k_f = 10^{-7}$ m/s, occur in depths $\geq$ 20 m below the foundation level. With the exception of the area situated directly under the foundation level, the dilatometer tests have provided Young's moduli ranging from 4.000 to 8.000 MPa. They did not show any dependence of depth.

In the masonry, two flat jack tests were carried out (fig. 7). The Young's modulus, deduced from test results for the rubble stone masonry, ranges from 8.000 to 12.000 MPa and is therefore higher than expected. The verifying analyses carried out later on do, however, confirm these values.

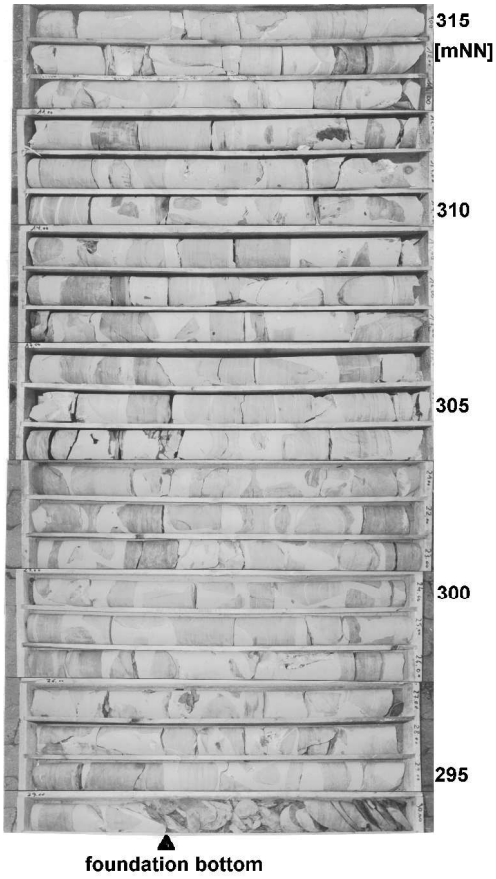

Fig. 5: Drill core KB 7 (masonry)

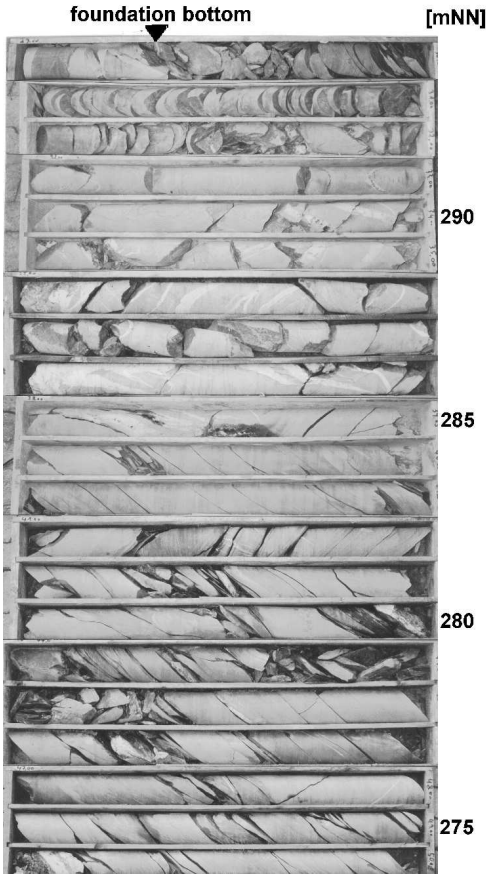

Fig. 6: Drill core KB 7 (rock)

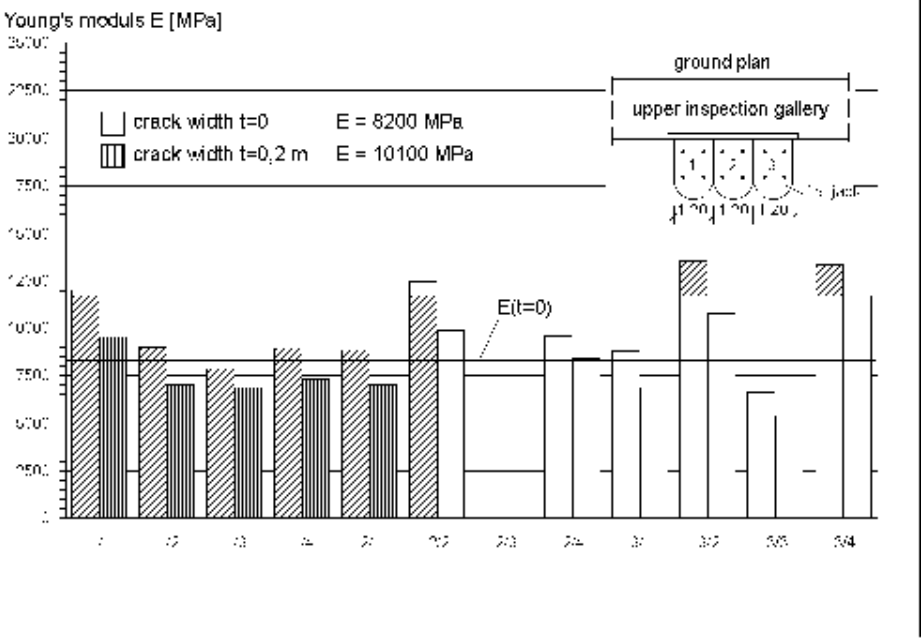

Fig. 7: Flat Jack Test 1 (horizontal) carried out in masonry
Young's moduli for crack widths of t=0 and t=0,2 m

3. Comparison of Monitoring and Analyses Results

The data gained from the extensive monitoring programme (fig. 2) were interpreted by means of three-dimensional finite element analyses using the three-dimensional FE-mesh shown in figure 8. Seepage flow analyses as well as stability analyses were carried out for the load cases dead weight of the dam impounding and temperature changes.

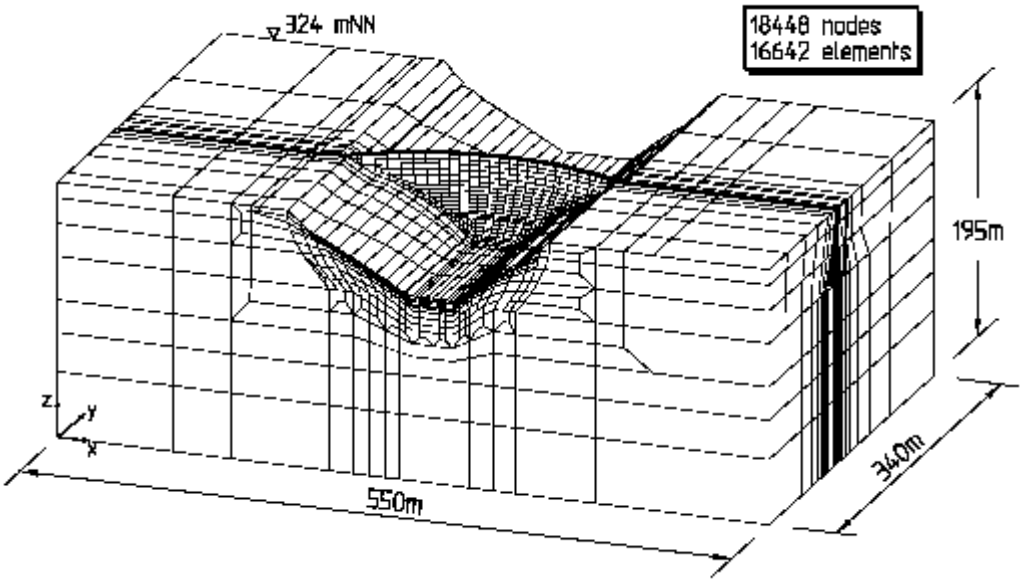

Fig. 8: FE-mesh, view from downstream

By means of a comparison of monitoring and analyses results and a variation of characteristic parameters for the masonry and the foundation rock, the finite element model was calibrated. Then, the calibrated model and realistic characteristic parameters were used to carry out the final stability analysis.

As an example for the pore water pressure measurements, figure 9 shows the monitoring results from measuring cross section VI for two different storage levels. These results illustrate the fast potential reduction from the water-side to the axis of the inspection galleries, which coincides with the axis of the fan of drainage holes, which was carried out in the dam. Moreover, it becomes clear that the foundation water pressure on the downstream side of the lower inspection gallery is determined by the storage level downstream of the dam.

Carrying out the seepage flow analysis for the calibration of the FE-model, the permeabilities of dam and rock have been varied until a good correspondence between measuring and analysis results was obtained. The result of this parameter variation is shown in figure 10 in form of potential lines and assumed permeabilities. A permeability coefficient of $k_f = 1 \cdot 10^{-6}$ m/s was determined for

the dam. For the underlying rock a graduation of permeability was defined. Up to a depth of 10 m below foundation level, a k_f-value of $8 \cdot 10^{-6}$ m/s was determined, for the rock in greater depth the k_f-value was set to $3 \cdot 10^{-7}$ m/s.

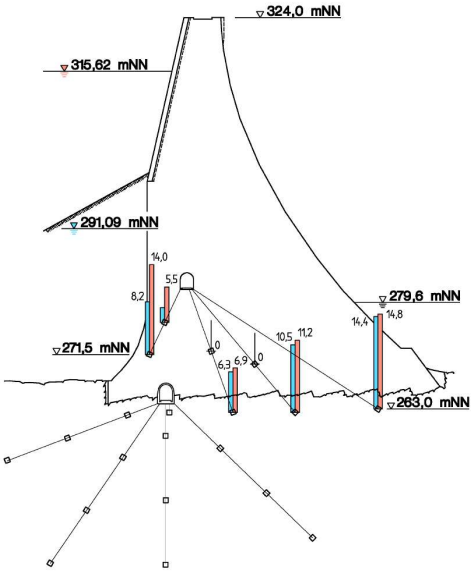

Fig. 9: Pore Water Pressure Measurements MQ VI

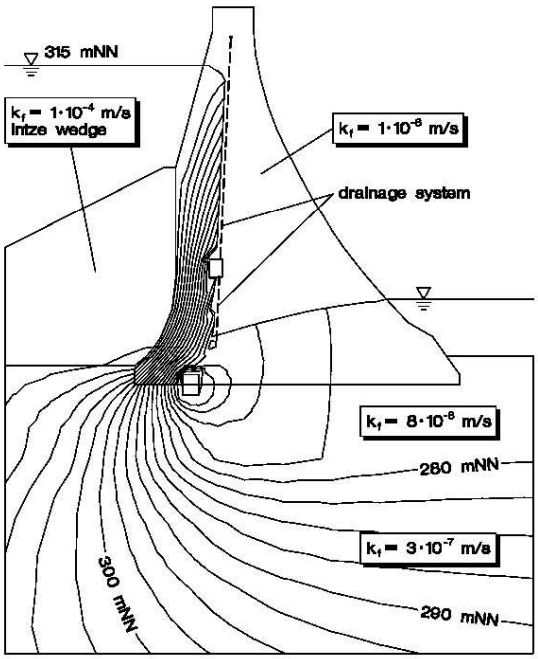

Fig. 10: Seepage Flow Analysis Equipotential Lines

After calibration of the model for seepage flow analysis and calculation of the resultants of the water pressure, the finite element model for the stability analyses was calibrated. For this, the displacement measurements (measurements of the displacements along the crest, pendulum and invetted pendulum as well as extensometers and inclinometers) were interpreted and, thereby, the dependance of the displacements on storage level and temperature changes was determined. Figure 11 shows the displacements derived from measuring results for a rise of the storage level from 295 m above sea level to 315 m above sea level and for a temperature increase of 10 °C (mean value of air and masonry temperatures). The rise of the storage level leads to a displacement of the dam's crest of 7 to 8 mm towards the downstream side. The rise in the dam's temperature leads to a displacement of 5 to 7 mm towards the upstream side.

The stability analyses were based on the characteristic values shown in figure 12. The Young's moduli of masonry and foundation rock were varied assuming, analogously to the seepage flow analysis, two rock zones with different compressibilities. The best coincidence with monitoring results was obtained

assuming a Young's modulus of 10.000 MPa for the masonry, of 4.000 MPa for the rock down to a depth of 10 m below foundation level and of 10.000 MPa for the rock in greater depth. Figures 13 and 14 show the displacements of the dam in the valley section and on the crest computed for this case. The computed displacements of the dam's crest of 6 mm approximately correspond with the measured values of 7 to 8 mm (fig. 11).

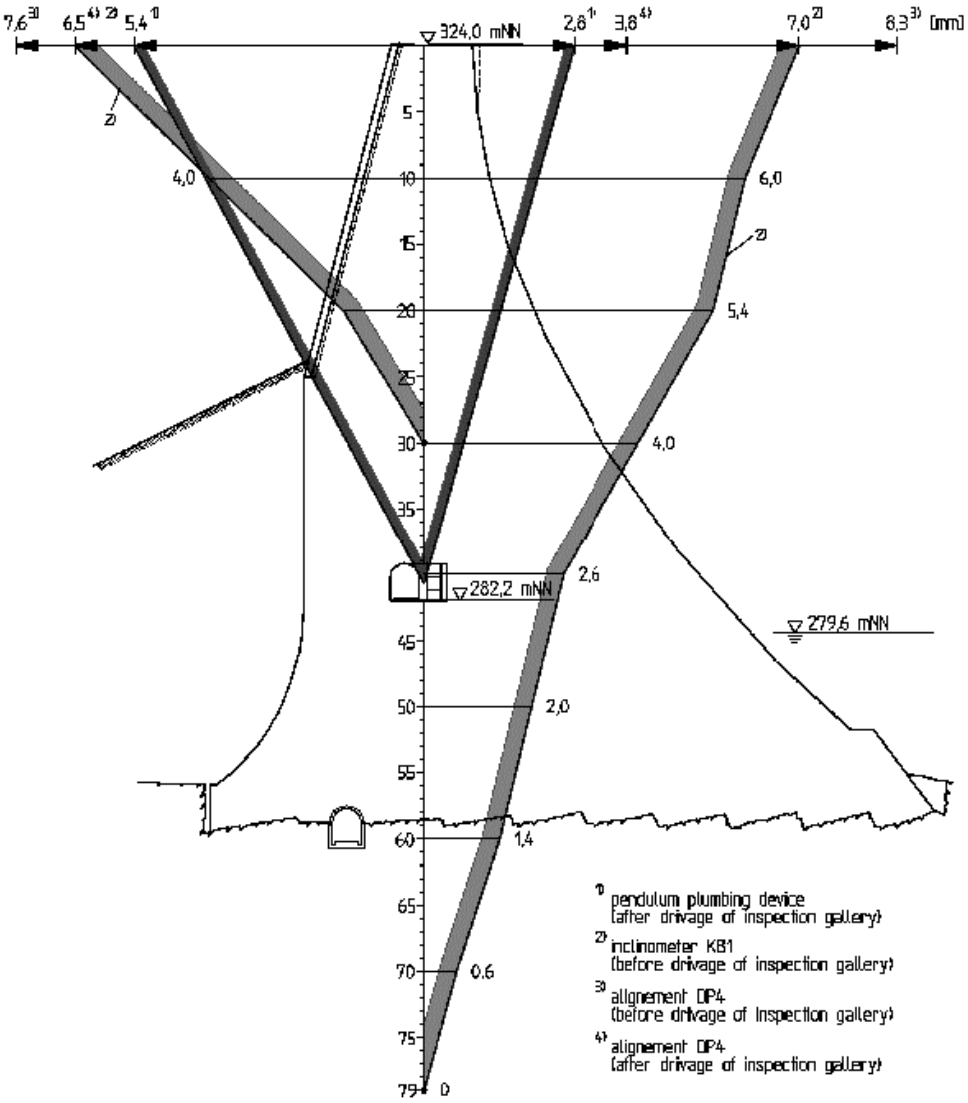

Fig. 11: Displacements of the Dam in Valley Midths caused by a Raise of Storage Level from 295 mNN to 315 mNN and by a temperature increase of 10° C

material		masonry		protection facing	rock mass	Intze-wedge
Young's modulus E [1])	[MPa]	s.b.		s.b.	s.b.	15
Poisson's ratio	[-]	0,25		0,25	0,35	0,4
unit weight	[kN/m³]	22		22	27	21
discontinuities						
orientation α / β	[°] / [°]	0/0	[2])/90	270/73,6	270/60	-
cohesion	[MPa]	10000	0	0	0	-
angle of internal friction φ	[°]	25	0	10	30	-
tensile strength β_z	[MPa]	0	0	0	0	-
dynamic E-Modulus	[MPa]	15000		-	15000	150
temperature coefficient α_T	[1/K]	$6 \cdot 10^{-6}$		$6 \cdot 10^{-6}$	-	-

1) variation of Young's modulus for calibration of the model: see below
2) radially orientated vertical discontinuities for the load case "dead weight"

Variation of parameters

	E-Modulus [MPa]		
Fall	masonry	rock mass, zone I slightly weathered	rock mass, zone II unweathered
A	8000	2000	8000
B	8000	4000	8000
C	10000	3000	8000
D	10000	4000	10000

Fig. 12: List of characteristic parameters for the stability analyses

Figure 15 shows the principal normal stresses in the dam for the design storage level, which is treated at 322,5 m above sea level.

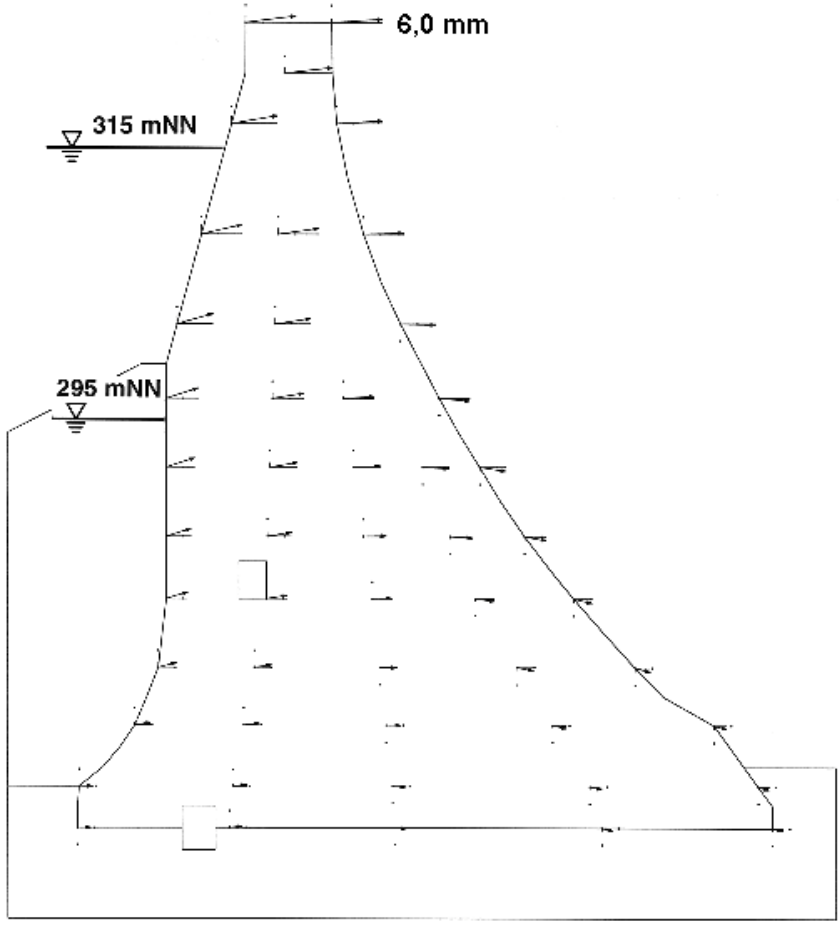

Fig. 13: Stability Analysis: Rise of Storage Level from 295 mNN to 315 mNN, Displacements caused by Rise of Storage Level

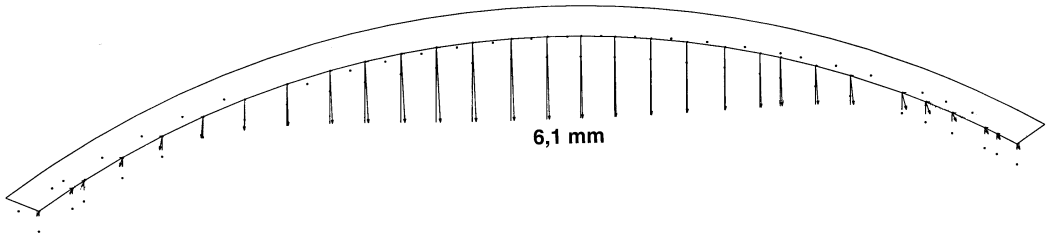

Fig. 14: Stability Analysis: Rise of Storage Level from 295 mNN to 315 mNN, Displacements caused by Rise of Storage Level, Top View on the Dam's Crest

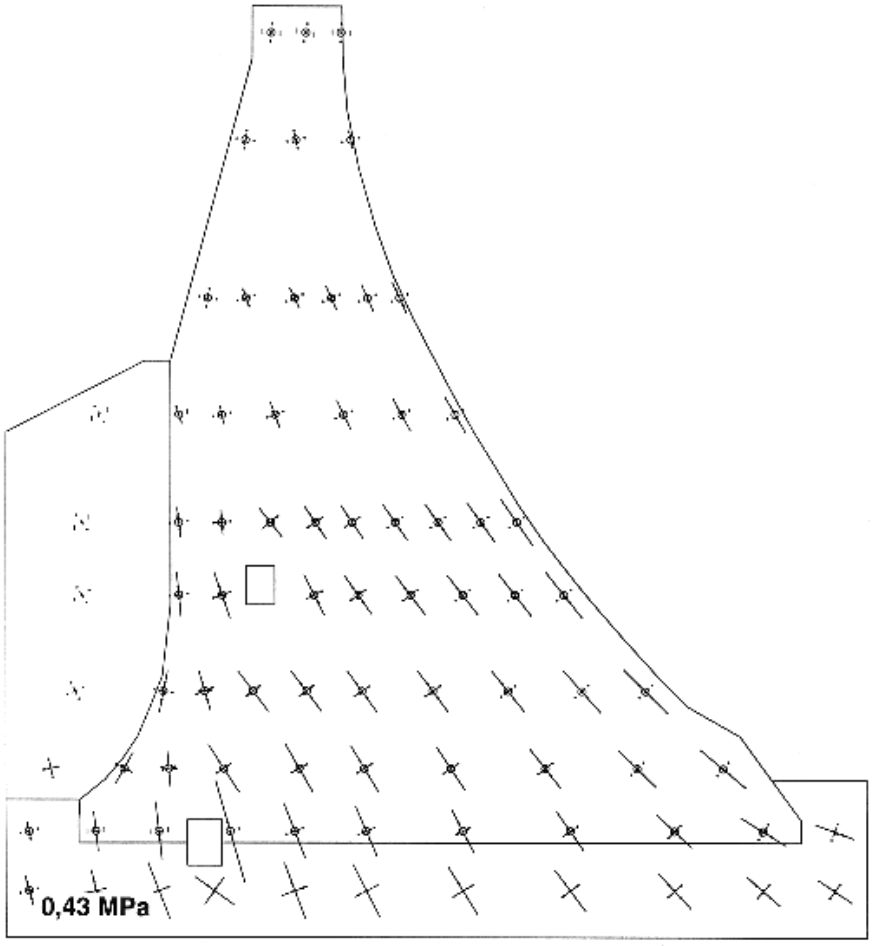

Fig. 15: Stability Analysis: Rise of Storage Level up to 322,5 mNN, Principal Normal Stresses in Valley Midth

In order to enable the numerical determination of the deformations of the dam caused by temperature changes, which amount to more than 20 °C throughout the year (fig. 16), the distribution of temperature in the dam is to be determined. For this, a total of 29 temperature gages were installed, equally distributed over the dam's section, in a measuring location in the middle of the valley (fig. 17). Then, the temperature distribution in the dam was deduced from the monitoring results. Figures 17 and 18 show the distribution of temperature in the dam during winter (lowest temperatures) and summer (highest temperatures). These temperature distributions were inserted into the finite element model and, thus, the deformations and stresses for the load case temperature were determined. Figures 19 and 20 illustrate the displacements resulting from the rise in temperature from winter to summer. The largest calculated displacement at the dam's crest of 6,5 mm coincides very well with the measured displacements of 5 to 7 mm (fig. 11).

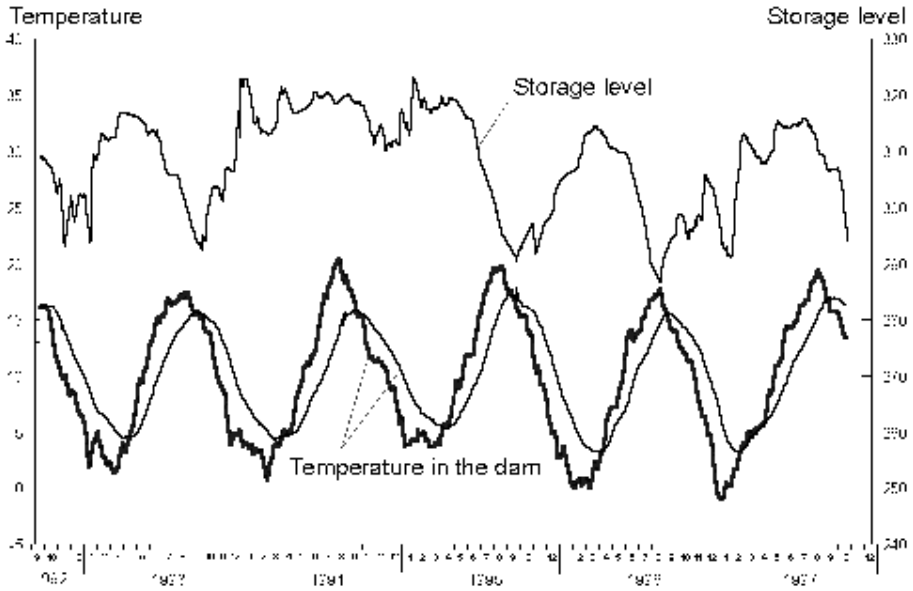

Fig. 16: Storage Level and Masonry's Temperature in the Area of the Dam's crest

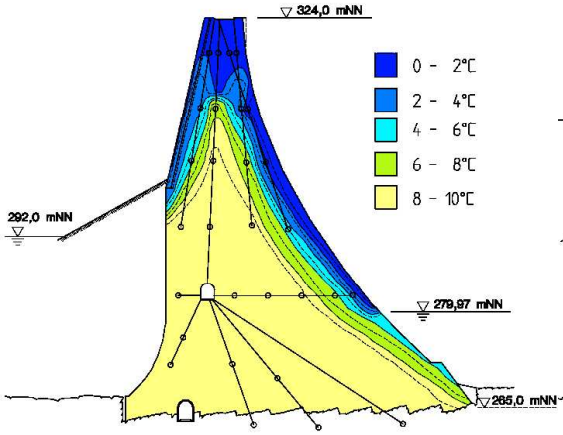

Fig. 17: Temperature Distribution in the Dam during Winter

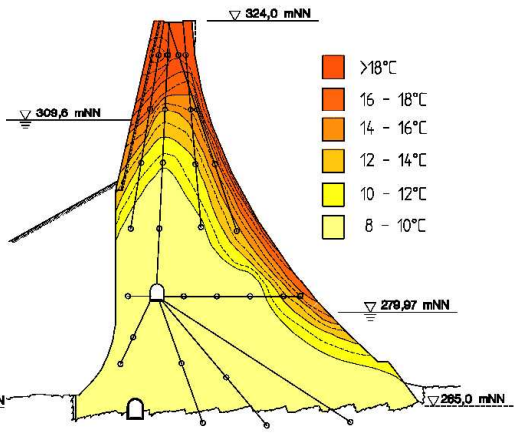

Fig. 18: Temperature Distribution in the Dam during summer

4. Conclusions

The extensive monitoring equipment installed in the Urft dam enables a reliable supervision of the structure as well as the calibration of the three-dimensional numerical model used to proof the stability of the dam. The stability analysis was carried out taking under consideration the loads resulting from dead weight, impounding and temperature changes. Moreover, analyses for the load case earthquake were carried out. Considering the threedimensional load-carrying action of the dam and using realistic characteristic values which had been

confirmed by measuring results, it could be shown with each analysis that the required stability of the dam is given. The realistic verification of the dam's load-carrying action and the good condition of the masonry enabled an economy-priced rehabilitation of the dam.

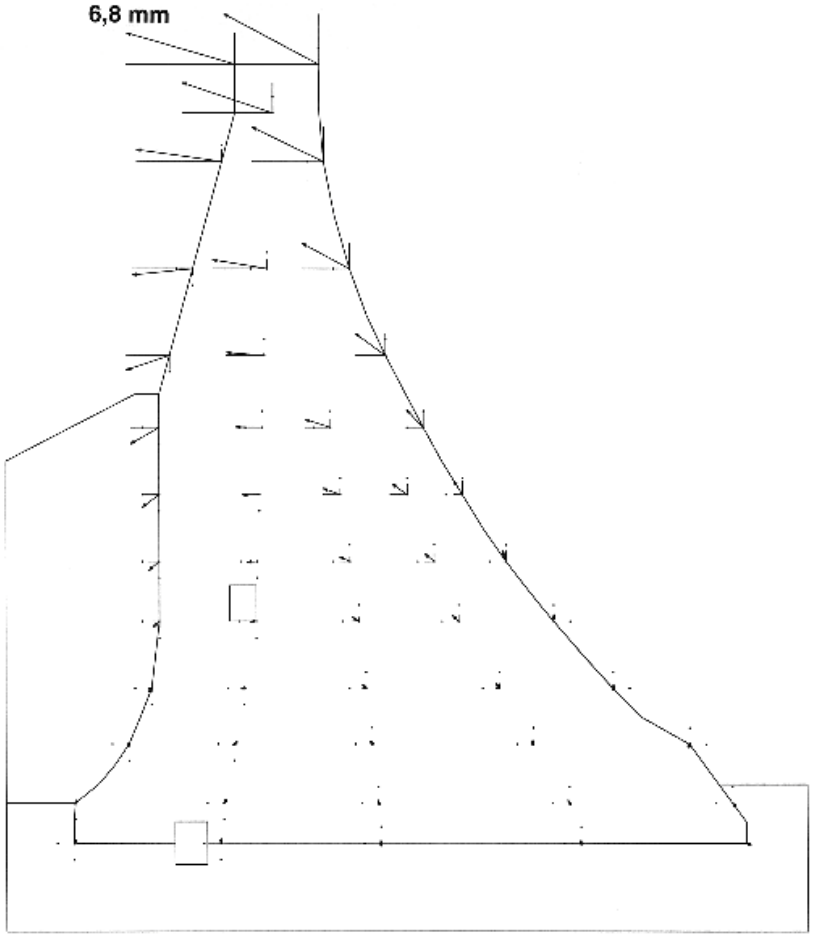

Fig. 19: Stability Analysis: Displacements in Valley Midth caused by Temperature Rise from Winter to Summer

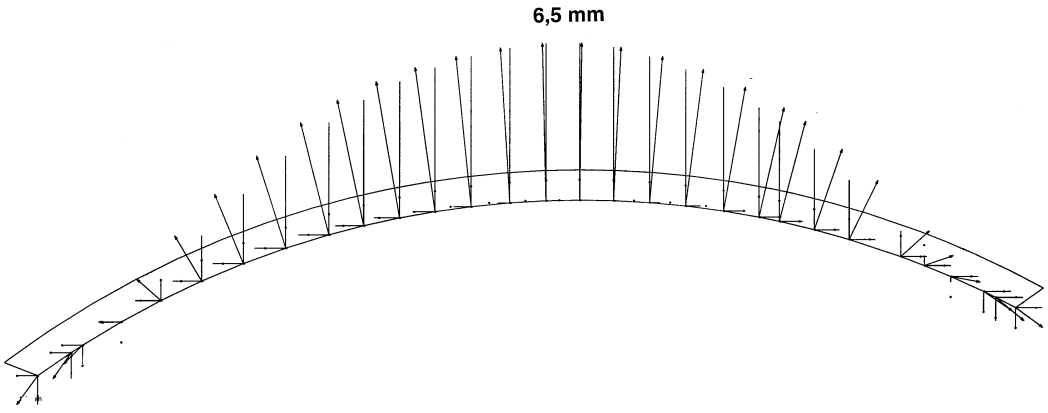

Fig. 20: Stability Analysis: Displacements at the Dam's crest caused by Temperature Rise from Winter to Summer

Literature

[1] DNK/DVWK: Talsperren in der Bundesrepublik Deutschland. Systemdruck GmbH, Berlin 1987.

[2] Wittke, W.: Rock Mechanics, Theory and Applications with Case Histories, Springer-Verlag, Berlin 1990.

[3] -WBI: Urfttalsperre, Zwischenbericht zu den Ergebnissen der Versuche und Messungen im Zeitraum September 1992 bis Oktober 1997, unveröffentliches Gutachten, Aachen, April 1998.

[4] WBI: Urfttalsperre, Standsicherheitsnachweis auf der Grundlage des Zwischenberichts vom April 1998, unveröffentlichtes Gutachten, Aachen, Mai 1998.

Summary

The 58 m high masonry dam of the Urft reservoir, which has a storage volume of approximately 45 Mio. m^3, was built around the turn of the century. Examining the dam's stability under consideration of today's standards, the stability was preliminary proven by means of a three-dimensional finite element analysis. In order to enable a concluding and reliable judgement of the dam's stability, inspection galleries were driven in the dam. Further monitoring devices were installed in various cross sections of the dam, and tests for determining mechanical and hydraulical parameters of the dam and the rock were carried out. Moreover, the existing drainage system was renewed and connected to the above mentioned galleries.

Based upon the test results and the comparison of monitoring and analysis results, a finite element model was elaborated, which enabled a realistic simulation of the load-carrying action of the dam and the underlying rock. Using this finite element model, the stability of the dam could be proven.